ADVANCED FUNCTIONAL MATERIALS
www.afm-journal.de

Materials Views
www.MaterialsViews.com

Template-Directed Liquid ALD Growth of TiO_2 Nanotube Arrays: Properties and Potential in Photovoltaic Devices

By *Thelese R. B. Foong, Yaodong Shen, Xiao Hu,** and *Alan Sellinger**

Dense and well-aligned arrays of TiO_2 nanotubes extending from various substrates are successfully fabricated via a new liquid-phase atomic layer deposition (LALD) in nanoporous anodic alumina (AAO) templates followed by alumina dissolution. The facile and versatile process circumvents the need for vacuum conditions critical in traditional gas-phase ALD and yet confers ALD-like deposition rates of 1.6–2.2 Å cycle^{-1}, rendering smooth conformal nanotube walls that surpass those achievable by sol–gel and Ti-anodizing techniques. The nanotube dimensions can be tuned, with most robust structures being 150–400 nm tall, 60–70 nm in diameter with 5–20 nm thick walls. The viability of TiO_2 nanotube arrays deposited on indium tin oxide (ITO)–glass electrodes for application in model hybrid poly(3-hexylthiophene) (P3HT):TiO_2 solar cells is studied. The results achieved provide platforms and research directions for further advancements.

1. Introduction

Well-ordered and vertically-aligned TiO_2 nanotube arrays on substrates are highly sought after for photovoltaic,[1,2] sensor,[3] and photocatalytic[4,5] applications primarily due to their directionality, high surface-to-volume ratios, and the ability to control their properties by varying nanotube dimensions. Fabrication routes to such arrays can be broadly categorized into self-directed and template-assisted approaches. Although self-assembly (including anodization of Ti[6] and hydrothermal growth procedures)[7] provides a more direct means to the arrays, template-assisted approaches[8,9] could prove better for more consistent control over nanotube dimensions as well as intertube spacings, which are required in certain applications.[10] Nanoporous alumina (AAO) from anodization procedures is highly favored as a template material for nanoparticle array deposition because the template formation process is straightforward[11–13] and results in a high density of parallel pore channels through which materials can be deposited.[14,15] For such reasons, AAO is the choice template material for our present study.

Atomic layer deposition (ALD) and sol–gel techniques are commonly used to deposit TiO_2 in AAO templates. ALD[16–20,9,21] is a vapor phase non-line-of-sight technique capable of producing highly conformal coatings even on substrates with complex features. However, like many vapor deposition techniques, ALD generally requires expensive equipment and high running costs incurred for vacuum conditions. The sol–gel approach is an attractive wet processing technique that provides wide area film coverage with simple and inexpensive apparatus. Chu et al.[8] produced TiO_2 nanotube arrays by immersing the templates (prepared on indium-tin-oxide (ITO)–glass) in TiO_2 sol for several minutes to fill the pore channels with sol particles. Although straightforward, the segregation of large gel particles during sol–gel transition and removal of large amounts of organic solvents during annealing often lead to high shrinkage, rendering conformal and crack-free nanotubes difficult to obtain.[22] Problems such as poor tube-to-substrate adhesion and variation in particle sizes over the height of the tubes were also identified.[8] Kunitake et al. developed a surface sol–gel (SSG) process[23,24] that has found several interesting applications such as nanoprecision replication of natural objects,[25,26] creation of defect-free dielectric films[22] and more recently, replication of AAO through-hole membranes creating unsupported TiO_2/polymer composite nanotubings in which a polymer was used as a binder to enhance mechanical properties.[27] Notably however, ALD has often been the choice technique to deposit TiO_2 nanotube arrays on substrates for reasons discussed above. Therefore, a more versatile and scalable method for nanotube array deposition could be desirable in proliferating the study of their material properties and the exploration of their potential applications.

Liquid-phase procedures that confer ALD-like conformal metal oxide coatings and yet circumvent the use of vacuum systems should bring significant benefits to the research community. In this work, we demonstrate the deposition of well-aligned TiO_2 nanotube arrays extending from Si and ITO–glass substrates by

[*] Prof. X. Hu, T. R. B. Foong, Y. D. Shen
School of Materials Science and Engineering
Nanyang Technological University (NTU)
Nanyang Avenue, 639798 (Singapore)
E-mail: asxhu@ntu.edu.sg
Prof. A. Sellinger[+]
Institute of Materials Research and Engineering (IMRE)
3 Research Link, 117602 (Singapore)
E-mail: aselli@stanford.edu
[+] Current address: Department of Materials Science and Engineering and the Center for Advanced Molecular Photovoltaics (CAMP), Geballe Laboratory for Advanced Materials, 476 Lomita Mall, Stanford, CA 94305-4045, USA

DOI: 10.1002/adfm.200902063

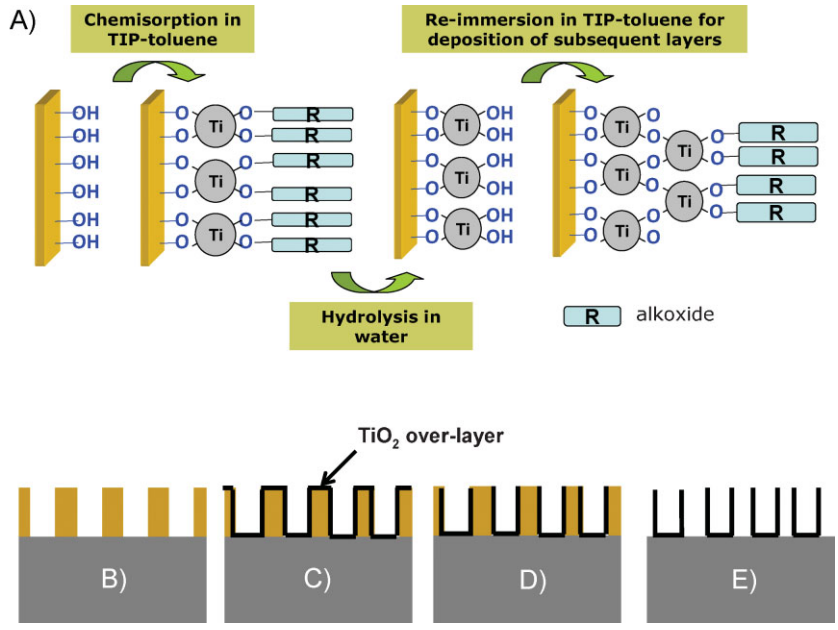

Scheme 1. Schematics of A) the sequential and repeated chemisorption/hydrolysis reactions in a typical LALD cycle and B–E) the formation of TiO_2 nanotubes by depositing in AAO templates prepared on substrates. TIP represents titanium(IV) isopropoxide.

precise "liquid-ALD (LALD)" replication (Scheme 1) of AAO templates fabricated directly on the substrates. We term our procedure "liquid-ALD" for we find the deposition rates and resulting films and nanostructures produced are strikingly similar to those from conventional gas-phase ALD, unachievable via sol–gel processes. Our intention is to develop a new facile LALD process that has the advantages of being more flexible, versatile, automatable, and scalable. We show that the rate of deposition has a direct influence on thin film morphology, which also dictates the ability to control the thickness and roughness of the nanotube walls. There are additional challenges in order to achieve uniform LALD deposition inside the nanochannels of the AAO templates on substrate where the bottom ends are closed. Furthermore, having recently overcome long-standing issues that have prevented the formation of AAO templates on ITO–glass,[28] we further explore the potential of the LALD-derived arrays for photovoltaic application by incorporating them in hybrid regioregular poly(3-hexylthiophene) (rrP3HT):TiO_2 excitonic solar cells. The arrays function particularly well for electron transport and result in efficiencies up to 0.3%.

2. Results and Discussion

2.1. Kinetics and Morphology of LALD Deposition

The kinetics of LALD deposition was monitored in real-time by subjecting a gold-coated quartz crystal microbalance (QCM) resonator to the sequential chemisorption/hydrolysis reactions. The thickness change per deposition cycle (d) was calculated using a derivative of the Sauerbrey equation, where ΔF is the frequency change observed and ρ is the density of TiO_2 powder (typically 1.7 g cm^{-3}):[24,23]

$$2d(\text{Å}) = \frac{-\Delta F(Hz)}{1.83\rho(\text{g cm}^{-3})} \quad (1)$$

Atomic force microscopy (AFM) images of thin films deposited on Si under similar experimental conditions were collected to correlate the rate of film growth to the resultant morphology. Immediate rinsing of substrates after chemisorption in titanium(IV) isopropoxide (TIP) with minimal exposure to humidity resulted in an almost constant growth rate of 2.4 Å cycle^{-1} (evident from the linearity of the QCM trend in Fig. 1A), and rendered films that were smooth and particulate-free at the sub-nanometer scale (Fig. 1B). Conversely deliberate prolonged exposure to the ambient generated films of inferior morphology (Fig. 1C). While a stable (but higher, 7.9 Å cycle^{-1}) growth rate (beyond 11 cycles, see arrow in Fig. 1A) could still be achieved, premature hydrolysis of excess reactants on the substrate resulted in the formation of large TiO_2 gel particles 15–20 nm in diameter across the substrate surface. Such observations suggest that with higher deposition rates, the deposition can no longer be considered a true ALD assembly, but instead approaches a typical sol–gel process. If translated to the nanochannels of the AAO template, premature hydrolysis would result in non-uniform nanotube wall thickness, which becomes an issue especially in a regime where

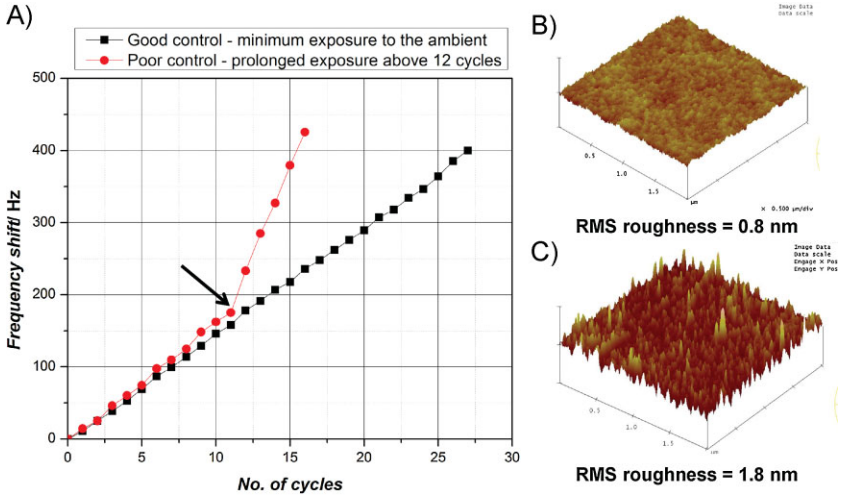

Figure 1. A) QCM frequency shifts ($-\Delta F$) as a function of the number of LALD deposition cycles. B,C) 3D AFM images of films deposited by 10 LALD cycles on Si substrates where B is a conformal film deposited with minimum exposure to the ambient and C is a film composed of particulates resulting from poor control over deposition conditions. RMS = root mean square.

size-dependent effects on the tube electronic structure are observed.[9] Moreover, the mass transport and loss of connectivity between the nanoparticles during crystallization[29] become significant and could impede charge transport in subsequent opto-electronic devices. The achieved deposition rate of 2.4 Å cycle^{-1} suggests an ALD-precise deposition. Transmission electron microscopy (TEM) analysis on the nanotubes leads to the same conclusion which is discussed in detail later.

2.2. Morphology and Crystal Structure in LALD-Derived TiO_2 Nanotube Arrays

Figure 2A,B show plan-view field-emission scanning electron microscopy (FE-SEM) images of AAO templates on Si before and after TiO_2 deposition, respectively. The pore openings are visibly smaller after deposition, but remain free of debris over all areas examined in this study, demonstrating the non-line-of-sight capability of the LALD technique. Dense and well-aligned arrays of nanotubes become apparent after template removal (Fig. 2C,D). X-ray photoelectron spectroscopy (XPS) scans (not shown here) indicated complete dissolution of AAO and also no traces of K^+ contamination from the KOH etchant. Arrays of nanotubes between 150 and 400 nm tall have been successfully produced. Nanotubes resulting from 30 deposition cycles have a wall thickness of ~5 nm (estimated from TEM), implying a deposition rate of approximately 1.6 Å cycle^{-1}. This value is similar to those published for conventional ALD in AAO templates (1.5–1.8 Å cycle^{-1}).[9] It is realized that achieving true ALD control is contingent on several critical factors including 1) a precursor that maintains its monomeric nature over the deposition process (which is a challenge due to its high reactivity), and 2) full conversion of the reactive groups during both precursor chemisorption and hydrolysis steps. In particular, the chemical composition of the hydrolysis bath had to be adjusted to ensure the repeatability of LALD in the confined AAO pore channels. Given its high surface tension, it was practically impossible for pure water to penetrate all the pore channels of the template to hydrolyze the chemisorbed alkoxide even with the help of ultrasonication. This resulted in nanotubes with varied wall thicknesses. The tubes with thicker walls that were left standing on substrate after template removal while those with thinner walls (due to inconsistent water penetration and hydrolysis), were weak and broke off from the substrate during the template removal process, leaving behind empty spaces amid clusters of standing tubes (Fig. 2E). A mixed solvent system was therefore used to tune the surface tension of the hydrolyzing medium. It was found that the use of ethanol hydrated with 10% water by volume for the hydrolysis step produced an array of tubes that was uniform across the substrate (Fig. 2C,D). The TEM image at low magnification (Fig. 2F) shows that the nanotube walls are relatively smooth, with no apparent segregation of large TiO_2 crystallites. The walls are also uniform in thickness along the length of the nanotube. A cluster of nanotubes with tube openings positioned parallel to the electron beam is shown in Fig. 2G.

While X-ray diffraction (XRD) results (Fig. 3I) suggest that the as-deposited nanotubes are amorphous, we have discovered through closer inspection by high-resolution TEM (at a suitably thin region near the nanotube opening, Fig. 3A) that they were in fact of a ''pseudocrystalline'' nature, in which there was already some degree of molecular ordering. The corresponding selected area diffraction (SAD) pattern (Fig. 3B) shows faint traces of diffraction rings. The observed ''pseudocrystallinity'' may be

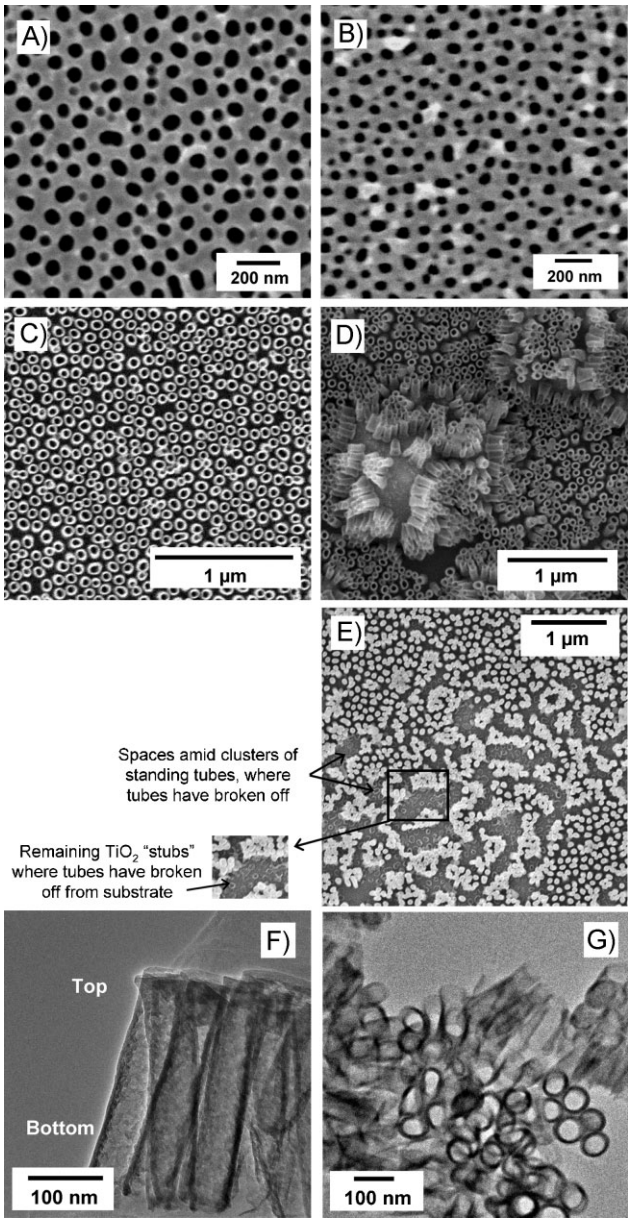

Figure 2. Plan view FE-SEM images showing the AAO template A) before and B) after LALD deposition. C,D) Plan view images of TiO_2 nanotube arrays on Si substrate after template removal. The nanotubes are ~150 nm tall, with an outer diameter of ~60–70 nm and wall thickness of ~5 nm. D) A cluster of dislodged nanotubes reveals the height of the tubes, the hollow tube channels, and the closed nanotube ends. E) Non-uniform array where tubes with thinner walls (due to inconsistent water penetration and hydrolysis) broke off from the substrate, leaving behind ''stubs'' (boxed regions). F,G) Low-magnification TEM images showing F) the full height of a cluster of TiO_2 nanotubes oriented perpendicular to the electron beam and G) a cluster of nanotube openings positioned parallel to the beam.

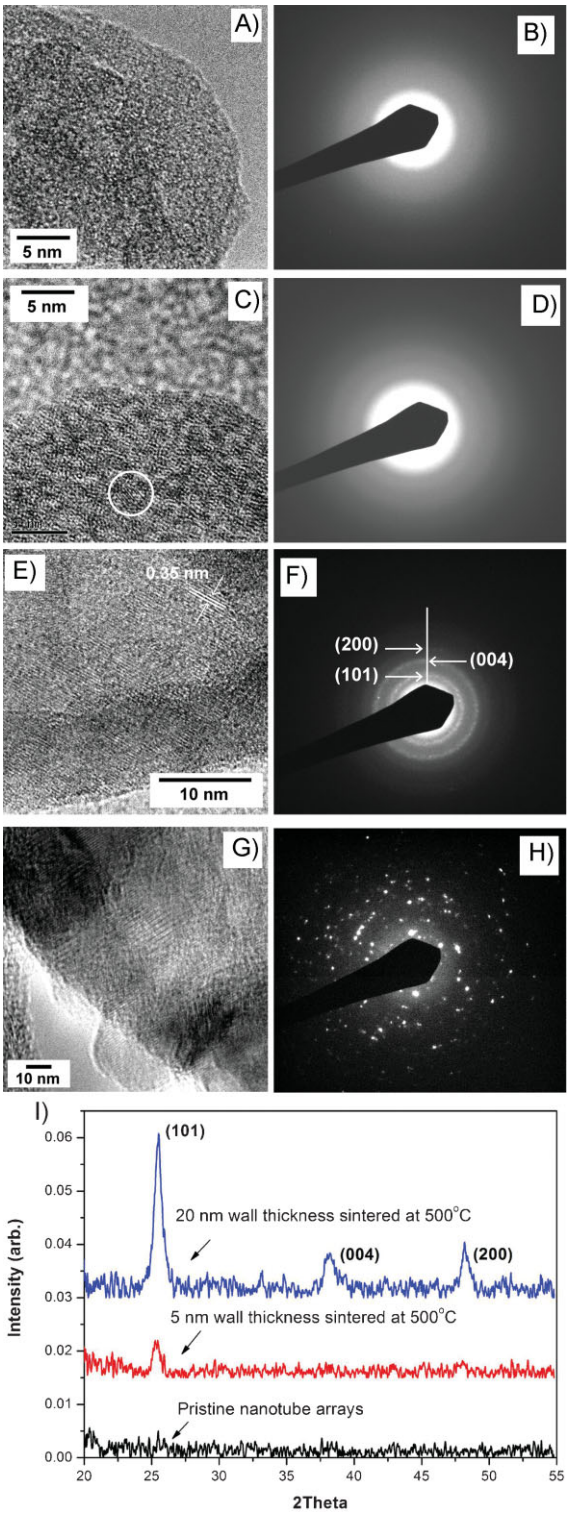

Figure 3. High-resolution TEM images of A) a pristine nanotube displaying "pseudocrystallinity" and B) its corresponding SAD pattern. The degree of crystallinity increases with nanotube wall thickness, with lattice fringes becoming progressively more prominent from C) 5 nm to E) 10 nm and G) 20 nm thick walls. The SAD pattern also progresses from D) faint to F) distinct rings and finally H) distinct spots. The increase in crystallinity is also evident from XRD analysis (I).

interpreted as evidence that our method is indeed a LALD layer-by-layer assembly. The degree of crystallinity in the arrays was found to increase with increasing nanotube wall thickness, in agreement with observations from the literature that crystallization in TiO_2 begins at a threshold thickness of 5 nm.[30] The XRD peaks and SAD ring pattern for nanotubes with wall thickness <5 nm (Fig. 3D,I) are poorly resolved with lattice fringes in small 2–3 nm domains that are barely detectable (see circled area in Fig. 3C). The crystallinity in nanotubes with 10 nm walls was improved with obvious lattice fringes extending over the length of the nanotubes (Fig. 3E). The lattice spacing of 3.5 Å corresponds to the distance between the primary anatase (101) crystal planes. Nanotubes with ~20 nm walls were fully crystalline and resulted in distinct SAD spots as well as XRD peaks (Fig. 3H and I, respectively). The lattice fringe images shown in Figure 3E,G indicate that single-crystal-like TiO_2 nanotubes were deposited. It is noted that the sol–gel derived TiO_2 is usually polycrystalline. Therefore, we believe the resultant single-crystal-like morphology should be a key attribute of LALD because such structure has not been reported in TiO_2 nanostructures prepared via sol–gel processes.

2.3. Photovoltaic Devices Incorporating the TiO_2 Nanotube Arrays

We next explored the potential of LALD-derived TiO_2 nanotube arrays as an n-type semiconductor in hybrid organic–inorganic solar cells. Widespread interests in the field of organic photovoltaics has been encouraged by the promise of an inexpensive renewable energy source manufactured via lower-cost and lower-energy-consuming techniques (e.g., high throughput roll-to-roll processing, spin/dip coating, printing and vacuum sublimation) than present silicon technology.[31] Of the many device architectures being pursued to achieve high efficiencies, the ordered bulk-heterostructure that features interdigitated donor and acceptor domains is expected to 1) improve further on exciton harvesting by providing donor–acceptor (D–A) interfaces within the exciton diffusion length-scale (3–10 nm) for charge dissociation, and 2) effectively minimize geminate recombination by providing direct charge percolation pathways to the electrodes (Fig. 4A).[10] TiO_2 nanotube arrays on ITO–glass electrodes such as those developed in this work (Fig. 4D) can serve as mechanically robust scaffolds for subsequent deposition and infiltration of a photo-active material resulting in the above device geometry.

Our model photovoltaic devices were composed of rrP3HT, the photon absorbing and exciton generating donor material, and the TiO_2 nanotube array which functions as the electron acceptor and transport medium (Fig. 4A). ITO–glass and Ag were the cathode and anode respectively. We adopted the melt-infiltration technique (used by Coakley et al. to deposit P3HT into the channels of mesoporous TiO_2[32,33] and empty AAO templates[34]) to promote the filling of P3HT into the nanotube arrays. Melt-infiltration involves depositing a layer of P3HT on the arrays and annealing at high temperatures (before metallization) to drive the polymer in under gravitational force. The efficiencies (η) of devices (with a 380 nm layer of P3HT) annealed in a N_2 atmosphere at temperatures ranging from 100–220 °C for 10 min are summarized in Figure 4B. In agreement with observations from the

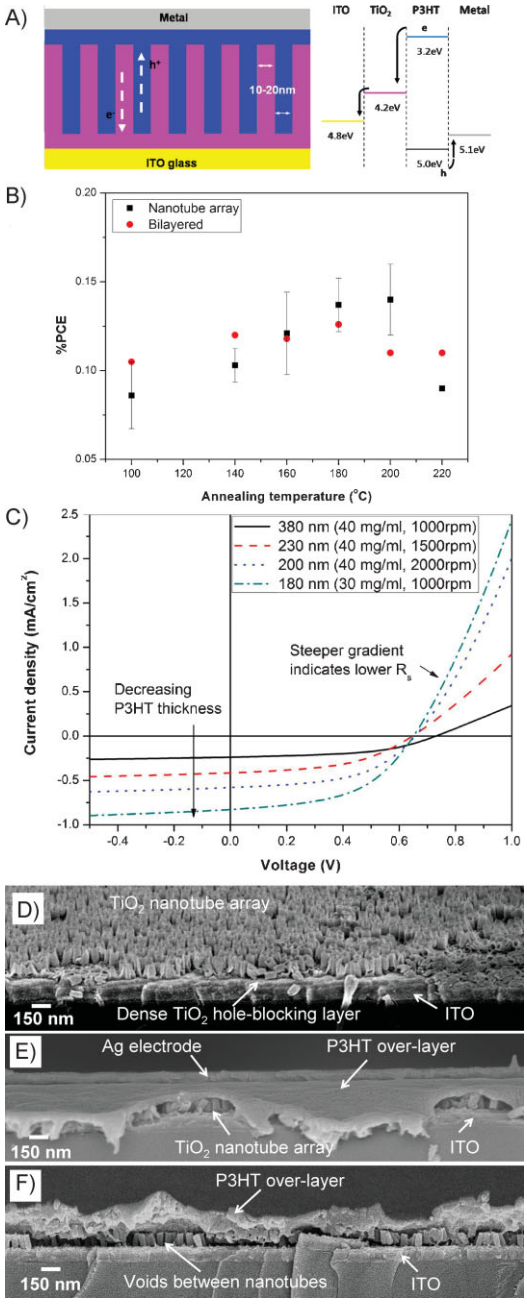

Figure 4. A) Schematic of an ideal device architecture featuring interdigitated donor and acceptor domains sandwiched between the two electrodes. The energy band diagram of a working P3HT:TiO_2 device is shown on the right. B) Power conversion efficiencies (PCE), η, of devices annealed (prior to metallization) at various temperatures to promote P3HT infiltration into the arrays. At temperatures above 160 °C, nanotube-based devices ■ begin to overtake the PCE of their bilayered counterparts ● as a result of better contacts between P3HT and the nanotubes forming. C) *I–V* curves of devices composed of TiO_2 nanotube arrays with various amounts of P3HT deposited on top. The nanotubes employed for device fabrication were 150 nm tall, 50–60 nm in diameter, spaced ~110 nm apart, had a wall thickness of ~10 nm, and were deposited on a 40 nm dense TiO_2 hole-blocking layer (D). Despite up to 6 h of melt infiltration at 200 °C, P3HT failed to infiltrate into the array as the cross-sectional FE-SEM images in E and F show.

literature, an annealing temperature of 200 °C resulted in devices with the highest η. Cross-sectional FE-SEM analyses (Fig. 4E,F) review partial P3HT infiltration. A number of modifications to device fabrication procedures have been evaluated to improve polymer filling. These include 1) prolonged annealing at 200 and 220 °C for up to 6 h, 2) soaking the nanotube arrays in pristine chlorobenzene and spinning dry prior to dispensing the P3HT solution, 3) dispensing and leaving the P3HT solution on the arrays for 1 min before spinning dry, and 4) functionalizing the surface of the arrays with a monolayer of octyltrichlorosilane (OTS) to convert the superhydrophilic nature of the nanotubes to a hydrophobic one for improving the compatibility between P3HT and the nanotubes.

The current–voltage (*I–V*) characteristics and key efficiency factors of several devices are presented in Figure 4C and Table 1. As expected, the short-circuit current (J_{sc}), fill factor (FF), and thus η improved with reduced P3HT thickness (adjusted by varying the concentration of P3HT in chlorobenzene and/or spin-coating speed) in tandem with reduced series resistance in the device (Fig. 4C). More significantly, over all thicknesses of P3HT, the J_{sc} resulting from nanotube arrays was higher than those from benchmark bilayer architectures based on featureless TiO_2 films (Table 1, within parentheses). The highest efficiency obtained (0.3%) is a twofold improvement over that of benchmark bilayered devices without the nanotube arrays. Such results are encouraging as they provide important proof-of-concept which can be further explored. For example, we plan to study the infiltration of small molecule and oligomeric donor materials to minimize the complexities associated with polymer infiltration. It is also interesting to work towards a better understanding of the orientation and charge transport properties in the polymer chains in the nanotube array.

3. Conclusions

In summary, we have demonstrated the practical feasibility of a liquid ALD (LALD) technique in preparing robust arrays of TiO_2 nanotubes extending from various substrates by the careful reaction of TiO_2 precursors on AAO templates. The process presents a facile, flexible automatable and scalable liquid-phase alternative to vapor-phase ALD. The methodology can be readily extended to other metal oxide systems or desired materials combination subject to the availability of suitable reactants and rinsing solvents. Furthermore, we demonstrated the potential of the TiO_2 nanotube arrays in hybrid P3HT:TiO_2 photovoltaic devices, in which the arrays functioned particularly well as an electron acceptor and conductor. We are currently working to better understand the driving forces behind polymer infiltration and chain orientation under nanoconfinement in the arrays.

4. Experimental

Preparation of Substrates for TiO_2 Deposition: AAO templates on Si and ITO–glass substrates were fabricated by anodizing Al films on the substrates. While Al (150–300 nm)-coated Si wafers were obtained commercially from Evaporated Coatings, Inc., those on ITO–glass (with sheet resistance of 10 Ω sq^{-1} obtained from Merck Display Technologies) were deposited by electron-beam evaporation (Edwards FL400) at a rate of 5 nm s^{-1}. Prior to Al deposition on ITO–glass, a dense layer of TiO_2 was

Table 1. Detailed efficiency factors of devices based on LALD-derived TiO_2 nanotube arrays and benchmark featureless films (within parentheses), where V_{oc} is the open-circuit voltage, J_{sc} is the short-circuit current density, and FF is the fill factor. The final PCE value is computed using the following formula: $PCE = (V_{oc} \times J_{sc} \times FF)/P_{in}$, where P_{in} is the power input from the solar simulator (100 mW cm^{-2}).

P3HT thickness	V_{oc} [V]	J_{sc} [mA cm^{-2}]	FF	η
380 nm (40 mg mL^{-1}, 1000 rpm)	0.73 (0.73)	0.39 (0.27)	0.37 (0.45)	0.11 (0.089)
230 nm (40 mg mL^{-1}, 1500 rpm)	0.65 (0.77)	0.41 (0.21)	0.47 (0.35)	0.15 (0.057)
200 nm (40 mg mL^{-1}, 2000 rpm)	0.65 (0.65)	0.58 (0.39)	0.52 (0.56)	0.20 (0.14)
180 nm (30 mg mL^{-1}, 1000 rpm)	0.65 (0.65)	0.82 (0.40)	0.50 (0.54)	0.30 (0.14)

spin-coated from a solution based on the acid-catalyzed hydrolysis of TIP in ethanol with a molar ratio of TIP/H_2O/ethanol/HNO_3 = 1:1:50:0.2 [35] and converted to anatase TiO_2 by sintering at 500 °C for 2 h in air. This TiO_2 layer (~40 nm) was vital to stabilizing the template formation process [28] as well as preventing shunt leakage in subsequent photovoltaic devices. The coated substrates were anodized opposite a platinum mesh counter electrode in oxalic acid (0.3 M) maintained at 2 °C, at voltages ranging from 40–60 V depending on the desired pore dimensions and spacing. They were then immersed in H_3PO_4 (5 wt%) for 30–75 min to remove the thin barrier layer at the bottom of the pore channels [14] and simultaneously adjust the pore diameter.

The kinetics of LALD assembly was monitored by recording the frequency change on a QCM after each deposition cycle. Gold resonators for QCM studies were degreased in acetone, rinsed with deionized (DI) water, immersed in Piranha solution (H_2SO:H_2O_2 = 3:1 by volume) and rinsed again with DI water. After drying with a N_2 blowgun, the resonators were left overnight in mercaptoethanol (10 mM in toluene) to functionalize the gold surface with reactive hydroxyl groups (Scheme 1), rinsed with ethanol and dried with the N_2 blowgun again. TiO_2 films were also deposited on Si substrates for morphological studies by AFM. The Si substrates were cleaned the same way as the gold resonators, but without the need for the mercaptoethanol functionalization step.

TiO_2 Thin Film and Nanotube Array Deposition: In a typical deposition cycle, QCM resonators or Si substrates were immersed in 100 mM of TIP (97% Aldrich) dissolved in anhydrous toluene for 3 min for the chemisorption reaction (Scheme 1a), followed by immediate sonication in isopropanol (IPA) to remove unreacted species. They were then immersed in DI water for 1 min to effect hydrolysis of the chemisorbed propoxide groups and dried with a N_2 gun. The above steps were repeated to obtain the desired film thickness. All reactions were performed under ambient conditions. To minimize the effects of humidity on the experiment, fresh TIP–toluene precursor solutions were used after every 10 deposition cycles.

TiO_2 nanotube arrays were formed by subjecting the AAO template (prepared on Si and ITO–glass substrates, Scheme 1b) to the above chemisorption, rinsing and hydrolysis steps, with three adjustments: 1) templates immersed in the chemisorption bath underwent brief ultrasonication before setting aside for 3 min, 2) hydrolysis was carried out in ethanol containing 10% DI water by volume, and 3) the templates were heated at 90 °C for 5 min before the next deposition cycle. Step 1 was essential to remove entrapped air pockets within the AAO pore channels and promote TIP filling. Step 2 was necessary for consistent water penetration and hydrolysis reaction in the nanoporous channels, while Step 3 enhanced the removal of excess moisture from the templates. Before the template could be chemically etched away to reveal the embedded nanotubes, it must be exposed by removing the over-layer of TiO_2 deposited on top of the AAO template (Scheme 1c). This was accomplished by a short reactive-ion etch using a gas mixture of CHF_3 (55 sccm) and O_2 (5 sccm), radio frequency (RF) power (175 W) and pressure (55 mTorr) in an Oxford Plasmalab80Plus etcher. The AAO template was dissolved by immersing in aqueous KOH (0.01 M) for 1 h (Scheme 1e) to leave behind the TiO_2 nanotube arrays extending from the substrate surface.

TiO_2 Nanotube and Thin Film Characterization: The TiO_2 nanotube arrays were characterized by FE-SEM (JEOL 6700F) at an acceleration voltage of 5 kV. XRD (Bruker GADDs) was performed to probe the crystal structure of the arrays. Individual nanotubes were studied by TEM (JEOL 2010 LaB6) operated at an acceleration voltage of 200 kV and filament current of 103 μA. Samples for TEM were prepared by gently scraping the substrates and dispersing the detached nanotubes in ethanol by ultrasonication. The suspension was then dispensed dropwise onto a TEM carbon grid and dried for observation. QCM data was recorded on the Princeton Applied Research QCM 917 and AFM images (in tapping mode) were collected on Digital Instrument's Nanoscope III. XPS analyses were conducted on the VG ESCALAB 220I-XL imaging system equipped with a monochromatic Al-α source.

Device Fabrication and Photovoltaic Measurements: Hybrid organic–inorganic solar cells composed of TiO_2 nanotube arrays infiltrated with rrP3HT (Fig. 4A) were fabricated by spin-coating P3HT dissolved in chlorobenzene on the arrays and annealing the films at 200 °C for 10 min to promote polymer infiltration and alignment (i.e., π–π stacking). The thickness of the P3HT over-layer was adjusted by varying the spin-coating speed and measured using cross-sectional FE-SEM after fabrication and characterization steps. The TiO_2 arrays were crystallized by sintering at 500 °C in air for 2 h prior to depositing P3HT. Following the evaporation of the top Ag electrode (both ITO and Ag were patterned to give pixel areas of ca. 0.14 cm^2), the completed devices were annealed further at 100 °C for 1 h to increase P3HT ordering within the pores and overlayer, and improve Ag-to-P3HT contact. Current–voltage curves, from which the PCE was computed, were recorded on a Keithley 2400 sourcemeter as the devices were placed under AM 1.5G simulated illumination from a KH Steuernagel solar simulator. The intensity of the simulator was adjusted with an NREL AM 1.5G-calibrated Si photodiode to address any mismatch between the spectral output of the simulator and the true terrestrial AM 1.5G solar insolation. All measurements were made in an N_2 filled glovebox with the AM 1.5G illumination channelled to the device through a quartz window in the glovebox.

Acknowledgements

The authors thank Nanyang Technological University (NTU) and the National Research Foundation (NRF) Singapore (NRF-G-CRP2007-01) for funding this work and the Institute of Materials Research and Engineering (IMRE) for extensive usage of laboratory facilities. We gratefully acknowledge Mr. Daniel T. H. Li (IMRE) for assisting with XPS data collection and analysis and Prof. Tim White (NTU) for helpful discussions on TEM characterization.

Received: November 3, 2009
Revised: December 11, 2009
Published online: March 11, 2010

[1] G. K. Mor, K. Shankar, M. Paulose, O. K. Varghese, C. A. Grimes, *Appl. Phys. Lett.* **2007**, *91*, 152111.
[2] G. K. Mor, O. K. Varghese, M. Paulose, K. Shankar, C. A. Grimes, *Sol. Energy Mater. Sol. Cells* **2006**, *90*, 2011.
[3] M. Paulose, O. K. Varghese, G. K. Mor, C. A. Grimes, K. G. Ong, *Nanotechnology* **2006**, *17*, 398.
[4] Y. K. Lai, L. Sun, Y. C. Chen, H. F. Zhuang, C. J. Lin, J. W. Chin, *J. Electrochem. Soc.* **2006**, *153*, D123.

[5] J. M. Macak, M. Zlamal, J. Krysa, P. Schmuki, *Small* **2007**, *3*, 300.
[6] C. A. Grimes, *J. Mater. Chem.* **2007**, *17*, 1451.
[7] Z. R. R. Tian, J. A. Voigt, J. Liu, B. McKenzie, H. F. Xu, *J. Am. Chem. Soc.* **2003**, *125*, 12384.
[8] S. Z. Chu, K. Wada, S. Inoue, S. Todoroki, *Chem. Mater.* **2002**, *14*, 266.
[9] M. S. Sander, M. J. Cote, W. Gu, B. M. Kile, C. P. Tripp, *Adv. Mater.* **2004**, *16*, 2052.
[10] K. M. Coakley, M. D. McGehee, *Chem. Mater.* **2004**, *16*, 4533.
[11] O. Jessensky, F. Muller, U. Gosele, *Appl. Phys. Lett.* **1998**, *72*, 1173.
[12] A. P. Li, F. Muller, A. Birner, K. Nielsch, U. Gosele, *Adv. Mater.* **1999**, *11*, 483.
[13] F. Y. Li, L. Zhang, R. M. Metzger, *Chem. Mater.* **1998**, *10*, 2470.
[14] M. S. Sander, L. S. Tan, *Adv. Funct. Mater.* **2003**, *13*, 393.
[15] S. Shingubara, *J. Nanopart. Res.* **2003**, *5*, 17.
[16] J. Aarik, A. Aidla, H. Mandar, V. Sammelselg, *J. Cryst. Growth* **2000**, *220*, 531.
[17] J. Aarik, A. Aidla, H. Mandar, T. Uustare, M. Schuisky, A. Harsta, *J. Cryst. Growth* **2002**, *242*, 189.
[18] J. Aarik, A. Aidla, T. Uustare, V. Sammelselg, *J. Cryst. Growth* **1995**, *148*, 268.
[19] M. A. Cameron, I. P. Gartland, J. A. Smith, S. F. Diaz, S. M. George, *Langmuir* **2000**, *16*, 7435.
[20] M. Ritala, M. Leskela, *Nanotechnology* **1999**, *10*, 19.
[21] L. K. Tan, M. A. S. Chong, H. Gao, *J. Phys. Chem. C* **2008**, *112*, 69.
[22] Y. Aoki, T. Kunitake, A. Nakao, *Chem. Mater.* **2005**, *17*, 450.
[23] I. Ichinose, H. Senzu, T. Kunitake, *Chem. Mater.* **1997**, *9*, 1296.
[24] I. Ichinose, H. Senzu, T. Kunitake, *Chem. Lett.* **1996**, 831.
[25] R. A. Caruso, *Angew. Chem. Int. Ed.* **2004**, *43*, 2746.
[26] J. G. Huang, T. Kunitake, *J. Am. Chem. Soc.* **2003**, *125*, 11834.
[27] J. Huang, T. Kunitake, *J. Mater. Chem.* **2006**, *16*, 4257.
[28] T. R. B. Foong, A. Sellinger, X. Hu, *ACS Nano* **2008**, *2*, 2250.
[29] B. Smarsly, D. Grosso, T. Brezesinski, N. Pinna, C. Boissiere, M. Antonietti, C. Sanchez, *Chem. Mater.* **2004**, *16*, 2948.
[30] L. E. Greene, M. Law, B. D. Yuhas, P. D. Yang, *J. Phys. Chem. C* **2007**, *111*, 18451.
[31] S. E. Shaheen, D. S. Ginley, G. E. Jabbour, *MRS Bull.* **2005**, *30*, 10.
[32] K. M. Coakley, Y. X. Liu, M. D. McGehee, K. L. Frindell, G. D. Stucky, *Adv. Funct. Mater.* **2003**, *13*, 301.
[33] K. M. Coakley, M. D. McGehee, *Appl. Phys. Lett.* **2003**, *83*, 3380.
[34] K. M. Coakley, B. S. Srinivasan, J. M. Ziebarth, C. Goh, Y. X. Liu, M. D. McGehee, *Adv. Funct. Mater.* **2005**, *15*, 1927.
[35] W. X. Que, A. Uddin, X. Hu, *J. Power Sources* **2006**, *159*, 353.